



Optimising PtFe nanoparticle structure to enhance catalytic activity and stability for propane oxidation

Zhenpeng Huang ^{a,1}, Jihang Yu ^{a,1}, Wenbo Li ^b, Xuan Tang ^{a,b}, Yanglong Guo ^a, Yun Guo ^a, Li Wang ^a, Sheng Dai ^b, Rui Liu ^c, Wangcheng Zhan ^{a,*}

^a State Key Laboratory of Green Chemical Engineering and Industrial Catalysis, Research Institute of Industrial Catalysis, School of Chemistry & Molecular Engineering, East China University of Science and Technology, Shanghai 200237, PR China

^b Key Laboratory for Advanced Materials and Feringa Nobel Prize Scientist Joint Research Centre, School of Chemistry & Molecular Engineering, East China University of Science and Technology, Shanghai 200237, PR China

^c State Key Laboratory of Environmental Chemistry and Ecotoxicology, Research Center for Eco-Environmental Sciences, Chinese Academy of Sciences, Beijing 100085, PR China



ARTICLE INFO

Keywords:

Bimetallic catalyst
Surface segregation
Propane oxidation
Active oxygen species
C-H bond cleavage

ABSTRACT

Although the development of highly active and stable platinum catalysts for the complete oxidation of hydrocarbons is crucial, there are still significant challenges that need to be addressed. Herein, the surface structure of PtFe nanoparticles (NPs) on PtFe/CeO_{2-x} ($x = \text{CO, H, O}$) catalysts was precisely tuned via thermal treatment in CO, H₂ and O₂ atmospheres. The structure of the PtFe NPs on the PtFe/CeO_{2-O} catalyst consisted of dispersed FeO_x nanoclusters anchored on the PtFe NPs core. As a result, the PtFe/CeO_{2-O} exhibited superior activity and water resistance for propane oxidation among all catalysts, which stems from the cooperation among robust metallic Pt sites, abundant active oxygen species, and FeO_x nanoclusters as additional sites for oxygen supply. However, the reaction path of propane oxidation was similar among the PtFe/CeO_{2-x} catalysts. This study offers encouraging insights for the deliberate development of robust and high-performing bimetallic catalysts to eradicate volatile organic compound pollutants.

Synopsis: The CeO₂-supported core-shell-like PtFe-FeO_x NPs catalyst synthesised via calcination treatment in oxygen atmosphere exhibits the excellent activity, good durability and water resistance for propane oxidation at low temperature.

1. Introduction

Volatile organic compounds (VOCs) are major contributors to fine particles and near-surface ozone pollutants generation in the atmosphere, which seriously threaten the environmental and human health [1–4]. An effective and promising method for removing VOCs is through catalytic oxidation, which offers advantages high efficiency at mild operating circumstances, no secondary emissions, and adaptability to a wide range of VOCs gas concentrations [5–7]. As members of VOCs, light alkanes (C₂-C₄) possess distinctive characteristics such as significant emissions and resistance to degradation due to their stable molecular structure and low polarisability [8–10].

Among a series of catalytic materials, Pt-based catalysts are regarded to be the most promising ones, and the metallic Pt or partially oxidised

Pt^{δ+} ($0 < \delta < 1$) is the most active site for C-H bond cleavage, which is generally considered to be the rate-limiting step for saturated hydrocarbon catalytic elimination [11–13]. However, the high cost of precious metals and suppression effect by water in exhaust gas severely hamper the vast range of applications for Pt-based catalysts. In particular, the catalytic efficiencies of Pt catalysts are vulnerable to deterioration under working conditions of high temperature, humidity, and oxygen concentration, as the Pt active species in metallic state are easily transformed into highly oxidised species under oxygen-rich reaction conditions, while the crystalline PtO₂ phase is inactive and water competes with reactants for available adsorption sites [8,14]. To date, strategies for the optimisation of carriers or the introduction of additives have been frequently adopted to strengthen the stabilisation of metallic Pt active phases. For instance, numerous studies have focused on

* Corresponding author.

E-mail address: zhanwc@ecust.edu.cn (W. Zhan).

¹ These authors contribute equally to this work.

utilising Nb_2O_5 , WO_3 , MoO_3 , and VO_x as support or additives in Pt catalysts due to their strong electrophilic character [15]. These additives prevent the active Pt^0 from being oxidised/deactivated and promote the adsorption of light alkanes during the reaction. However, the hydrophilic character of these additives can inhibit the H_2O resistance of the modified catalysts [16–18]. Additionally, acid modification of the supports can efficiently prompt C-H bond scission through the construction of the dipolar catalytic site, but the redox property of the catalyst inevitably deteriorates owing to the blockage of oxygen defect sites and the suppression of lattice oxygen mobility [8,11]. Therefore, the construction of a robust metallic Pt site with high water resistance in monometallic Pt catalysts for catalytic oxidation of C_3H_8 is quite problematic because of the mutual exclusivity of these qualities and scarcity of alterable parameters.

In contrast to their monometallic counterparts, bimetallic Pt-M (M=transition metal) catalysts not only reduce the amount of precious metals, but their activities and stabilities can also be significantly enhanced owing to electronic effects, interface confinements and synergistic effect [19–22]. Recently, the dual-active site effect of Pt-MO_x in bimetallic catalysts has received considerable research attention for hydrocarbon oxidation. For examples, Tahsini et al. prepared the $\text{Pt}_x\text{Cu}_{100-x}$ catalysts with similar size but different composition through the colloidal method for propene combustion. The $\text{Pt}_x\text{Cu}_{100-x}$ catalysts with 15–30 at. Cu% exhibited the higher activity compared to pure Pt, which was related to the tuning of the electronic structure of Pt by Cu modifications to reach optimal binding energies of C^* and O^* intermediates [19]. Similarly, Shan et al. developed $\text{PtNiCo/Al}_2\text{O}_3$ catalyst for total oxidation of hydrocarbons and excellent activity and thermal stability in propane oxidation in comparison with Pt, which was derived from the oxygenated Pt-NiOCO₀ surface layer functioned as an oxygen reservoir for oxygen activation [23]. More importantly, structural turning of bimetallic NPs through selective leaching, multistep fine synthesis, and post-synthetic treatment would efficiently improve their catalytic performances [20–22]. For example, annealing bimetallic catalysts in an oxidizing or reducing environments can tune the atomic structure of bimetallic NPs by selective migration of metal and enhance the activity of bimetallic catalysts, due to the different binding abilities of metal elements with adsorbent molecules under the given conditions, which is often called the adsorbate-induced surface segregation strategy [24–26]. Therefore, the bimetallic catalysts have significant potential in constructing a highly active and robust catalyst for catalytic oxidation of C_3H_8 .

In this study, wormlike PtFe NPs were successfully synthesised using a wet-chemistry method and loaded onto a CeO_2 support with a high oxygen storage/release capacity. After subsequent thermal treatment in CO, H_2/Ar , and O_2/Ar atmospheres based on the adsorbate-induced surface segregation strategy, the surface layer composition of the PtFe NPs was tuned from a Pt skin shell and the random distribution of Pt and Fe to an FeO_x -rich surface. Consequently, the CeO_2 -supported core-shell-like PtFe- FeO_x NPs catalyst after post-treatment in an O_2/Ar atmosphere not only shows excellent catalytic activity for propane oxidation, but is also stable and resistant to water poisoning. This outstanding performance was mainly attributed to the cooperation of robust metallic Pt sites, abundant active oxygen species, and FeO_x nanoclusters, which acted as additional oxygen reservoirs for the reaction.

2. Experimental

2.1. Catalyst preparation

2.1.1. Synthesis of PtFe NPs

The PtFe nanoalloy was prepared using a colloidal chemical method described in the literature [27]. Briefly speaking, 0.5 mmol of $\text{Fe}(\text{acac})_3$, $\text{Pt}(\text{acac})_2$, and 20 mL of oleylamine were first mixed in a four-necked flask and sonicated for 5 min at room temperature. Then, the mixtures were magnetically stirred and heated at 80 °C for 30 min under a gentle

flow of N_2 . Next, the solution was further heated to 300 °C at 3 °C/min and kept at 300 °C for 1 h. The NPs were precipitated and separated by adding a hexane/ethanol mixture and centrifugation at 8500 rpm for 8 min, and the obtained precipitate was washed at least twice to remove the organic impurities and precursor residues. The actual yield of PtFe NPs through the colloidal method is 87.5% by calculating the ratio of the actual mass to the theoretical mass of PtFe NPs. Finally, the PtFe NPs were redispersed in hexane and kept in a low-temperature environment.

2.1.2. Preparation of $\text{PtFe}/\text{CeO}_{2-x}$ catalyst

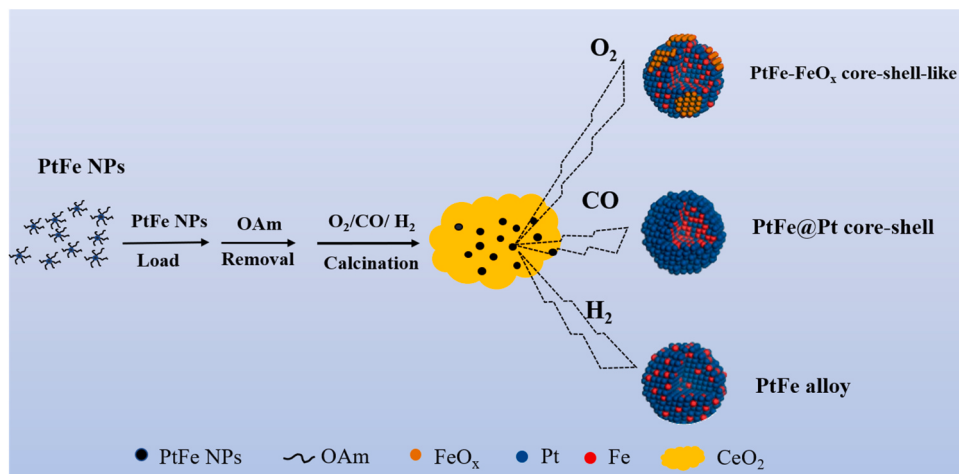
The PtFe NPs were deposited on the CeO_2 support by solution-phase adsorption-assisted assembly. Specifically, the CeO_2 NPs were obtained by calcining the $\text{Ce}(\text{NO}_3)_3 \cdot 6 \text{H}_2\text{O}$ precursor in air at 500 °C for 4 h, and the 500 mg of CeO_2 was first mixed with 20 mL of hexane and sonicated for 20 min. Next, a certain amount of PtFe NPs was slowly added dropwise into the CeO_2 powder dispersion under magnetic stirring. The content of Pt and Fe in the liquid after NPs deposition was below the limit of ICP-AES detection, indicating that the PtFe NPs dispersed in hexane solvent can be completely deposited on surface of CeO_2 support. Subsequently, the mixture was centrifuged and washed twice with ethanol (denoted as PtFe/CeO_2). Finally, the surfactant bonded to the PtFe NPs on the PtFe/CeO_2 surface was removed by hydrazine hydrate extraction [20]. Finally, the $\text{PtFe}/\text{CeO}_{2-x}$ ($x = \text{H, CO, or O}$) were calcined under 5 vol% H_2/Ar , pure CO, and 20 vol% O_2/Ar atmospheres at 400 °C for 1 h with a flow rate of 20 mL/min to regulate the PtFe NPs surface compositions based on adsorbate-induced surface segregation. Besides, the actual contents of Pt and Fe in the $\text{PtFe}/\text{CeO}_{2-x}$ catalyst were 1.1 wt% and 0.34 wt%, respectively, as detected by ICP-AES. An illustrated description of the preparation procedure is shown in [Scheme 1](#). Besides, the PtFe/SiO_2 catalysts were synthesized by a similar preparation method to that of the PtFe/CeO_2 catalyst. The Pt/CeO_2 catalyst was synthesized as a control sample, and the Pt NPs were prepared using a colloidal chemical method described in the literature [28]. Meanwhile, $\text{Pt}/\text{CeO}_2\text{-IMP}$, $\text{Fe}/\text{CeO}_2\text{-IMP}$ and $\text{PtFe}/\text{CeO}_2\text{-IMP}$ were prepared by incipient wetness impregnation method. The specific preparation process is described in [Supporting Information \(SI\)](#).

2.2. Catalysts characterization

The structural and physicochemical properties of the prepared catalysts are characterized, including N_2 adsorption and desorption, Raman spectra, powder X-ray diffraction (XRD), Inductively coupled plasma atomic emission spectroscopy (ICP-AES), X-ray photoelectron spectroscopy (XPS), Transmission electron microscopy (TEM), High-angle annular dark-field scanning transmission electron microscopy (HAADF-STEM), Energy-dispersive X-ray spectroscopy (EDS) mapping, Temperature-programmed desorption of O_2 ($\text{O}_2\text{-TPD}$), Temperature-programmed reduction by H_2 ($\text{H}_2\text{-TPR}$), Fourier transform infrared spectroscopy (FTIR), Propane adsorption and oxidation followed by Diffuse Reflection Fourier Transform Infrared Spectroscopy (DRIFTS). The details are described in the [SI](#).

2.3. Catalytic activity testing

The propane oxidation tests on the prepared catalysts were carried out in a fixed-bed quartz microreactor. Specifically, 100 mg of the catalyst was used, and the feed gas consisted of 0.2 vol% C_3H_8 , 2 vol% O_2 and 97.8 vol% Ar with a total gas flow rate of 50 $\text{mL}\cdot\text{min}^{-1}$ and weight hourly space velocity (WHSV) of 30000 $\text{mL}\cdot\text{h}^{-1}\cdot\text{g}_{\text{cat}}^{-1}$. The C_3H_8 conversion was calculated according to the formula $X_{\text{C}_3\text{H}_8} = ([\text{C}_3\text{H}_8]_{\text{in}} - [\text{C}_3\text{H}_8]_{\text{out}})/[\text{C}_3\text{H}_8]_{\text{in}}$, where $[\text{C}_3\text{H}_8]_{\text{in}}$ and $[\text{C}_3\text{H}_8]_{\text{out}}$ are the inlet and outlet C_3H_8 concentrations, respectively. The CO_2 selectivity was close to 100%, and no by-products other than CO_2 and H_2O were detected. The detailed activity and kinetic tests are provided in [SI](#).



Scheme 1. Schematic of the preparation process of the PtFe/CeO₂-x catalysts with different structures.

3. Results and discussions

3.1. Catalytic performance evaluation

3.1.1. Catalytic activities for C₃H₈ oxidation

The propane oxidation activities over PtFe/CeO₂-x catalysts during successive reactions were presented in Fig. S1. The propane activities of PtFe/CeO₂-O catalyst remained unchanged during three successive reactions, but those of the PtFe/CeO₂-H and PtFe/CeO₂-CO gradually increased and decreased in the three successive reactions, respectively. Notably, the catalytic activity of all PtFe/CeO₂-x catalysts kept stable after three successive reactions. The different evolution of the catalytic performances for the PtFe/CeO₂-x catalysts in the oxidation of propane during successive reactions was attributed to the structural evolution of PtFe NPs in the catalysts under an oxygen-rich reaction atmosphere. Therefore, the catalysts were used for subsequent testing and characterisation after the third cycle.

Propane conversion over PtFe/CeO₂-x catalysts is shown in Fig. 1A. It was noted that the CO₂ selectivity was almost 100% over all PtFe/CeO₂-x catalysts during the propane oxidation (Fig. S2). CeO₂ support showed a very poor propane oxidation activity, with only 30% conversion at 400 °C. However, the loading of PtFe NPs greatly enhanced the activity of the catalysts. The T₉₀ (the reaction temperature for 90% conversion of C₃H₈) order of the catalytic activity was as follows: PtFe/

CeO₂-O (280 °C) < PtFe/CeO₂-H (315 °C) < PtFe/CeO₂-CO (340 °C). Additionally, the oxidation rates and turnover frequencies (TOFs) of PtFe/CeO₂-x catalysts were determined at 200 °C (Table S1). Specifically, the PtFe/CeO₂-O catalyst demonstrated the highest reaction rate (15.1×10^{-6} mol_{C3H8}•g_{Pt}⁻¹•s⁻¹) and TOF (0.014 s⁻¹) followed by the PtFe/CeO₂-H (6.89×10^{-6} mol_{C3H8}•g_{Pt}⁻¹•s⁻¹ and 0.0053 s⁻¹) and the PtFe/CeO₂-CO catalysts (4.62×10^{-6} mol_{C3H8}•g_{Pt}⁻¹•s⁻¹ and 0.0031 s⁻¹). Meanwhile, the reversed order of the activation energy (Ea) of PtFe/CeO₂-O (43.4 kJ/mol) < PtFe/CeO₂-H (59.1 kJ/mol) < PtFe/CeO₂-CO (68.6 kJ/mol) (Fig. 1B) also demonstrated that the catalytic activity order of PtFe/CeO₂-O > PtFe/CeO₂-H > PtFe/CeO₂-CO. A performance comparison between the PtFe/CeO₂-O catalyst and the other catalysts reported in the literature is presented in Table S2. The catalytic performance of the PtFe/CeO₂-O was superior to that of most other catalysts, including commercial Pt/γ-Al₂O₃ and Pt/Ce-Zr (Fig. S3), indicating that the PtFe/CeO₂-O catalyst is an excellent oxidative catalyst for the removal of alkane pollutants.

Besides, considering that fluctuating concentrations and gas flows are frequent in industrial VOC emissions, the catalytic performance of the PtFe/CeO₂-O catalyst was further investigated under various conditions for the purpose of evaluating the applicability of the catalyst. The PtFe/CeO₂-O catalyst was still found to maintain its excellent catalytic performance even at the high gas flow of 60000 mL·h⁻¹·g_{cat}⁻¹, and the T₉₀ was 300 °C compared to a value of 280 °C at GHSV = 30000 mL·h⁻¹·g_{cat}⁻¹ (Fig. S4).

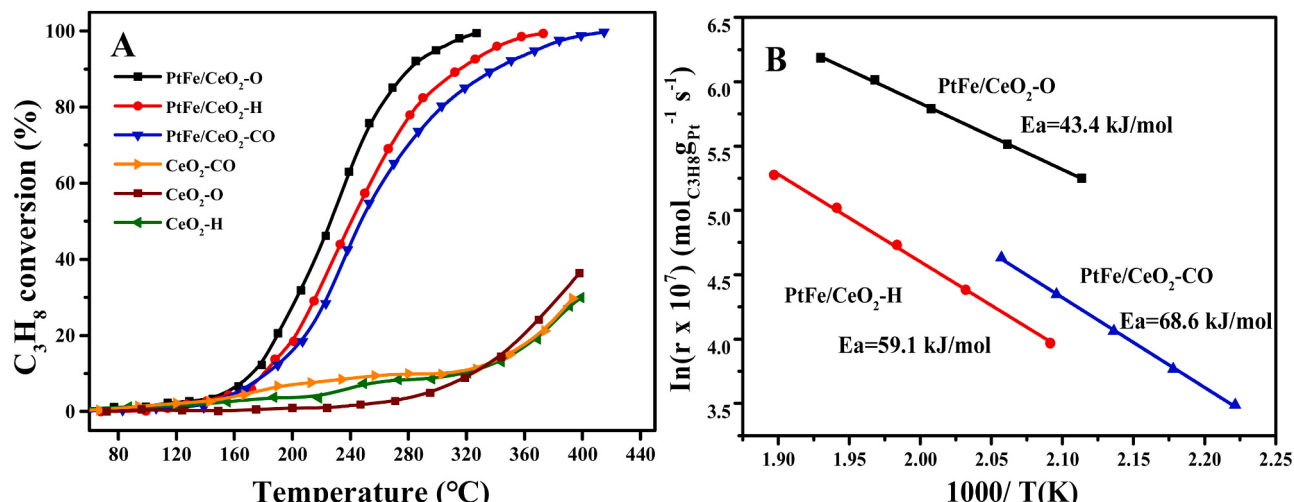


Fig. 1. (A) Propane conversion curves over PtFe/CeO₂-x catalyst at GHSV = 30000 mL·h⁻¹·g_{cat}⁻¹ and (B) the Arrhenius plots and fitted Ea of propane oxidation at GHSV = 150,000 mL·h⁻¹·g_{cat}⁻¹. Reaction conditions: 0.2 vol% of C₃H₈, 2 vol% of O₂ with Ar as balance gas.

On the other hand, as the C_3H_8 concentration in the feed gas increased from 500 to 2500 ppm, the C_3H_8 conversion over the PtFe/CeO₂-O catalyst gradually increased (Fig. S5). Meanwhile, the PtFe/CeO₂-O maintains good propane oxidation activity even under 20% oxygen reaction conditions, indicating that the PtFe/CeO₂-O catalyst exhibits high adaptability to the concentrations of both pollutants and oxygen. In short, the PtFe/CeO₂-O catalyst showed good oxidation activity and durability for propane oxidation.

3.1.2. Catalyst water resistance and stability

Meanwhile, taking into account the presence of water vapour under the real working condition, the water resistance tests over the PtFe/CeO₂-x catalysts were investigated at 285 °C (Fig. 2A). The propane oxidation activity of the PtFe/CeO₂-O catalyst was slightly decreased when 5 vol% of H₂O was introduced to the feed gas. However, the activities of both the PtFe/CeO₂-H and PtFe/CeO₂-CO catalysts significantly decreased and were comparable when introducing 5 vol% H₂O in the feed gas. The CO₂ selectivity over the PtFe/CeO₂-x catalysts were close to 100% for propane oxidation under wet conditions (Fig. S6). Moreover, the oxidation activity of the PtFe/CeO₂-O catalyst remained stable after multiple successive light-off (Fig. 2B) under humid conditions. These results demonstrated that the PtFe/CeO₂-O catalyst has better resistance to water than the other two catalysts.

In addition to the requirements for high catalytic activity, the stability of the catalyst is also a crucial parameter in practical applications.

In Fig. S7, no obvious deactivation was observed on all PtFe/CeO₂-x catalysts within a reaction time of 30 h under dry conditions. Besides, the effect of water content in the feed gas on the stability over the PtFe/CeO₂-O catalyst was further investigated (Fig. 2C). The conversion of C_3H_8 over the PtFe/CeO₂-O catalyst was stabilised at 95% initially, and was slightly decreased to 88% and 84% when adding 5 vol% and 10 vol% H₂O in the feed gas, respectively. However, the C_3H_8 conversion dropped significantly from 80% to 69% and 62% over Pt/CeO₂ in the presence of 5.0 and 10 vol% water vapour, respectively. H₂O in the reaction feed generally inhibited the oxidation reaction due to its competing adsorption with reactant molecules on the active sites. As for the Pt/CeO₂ and PtFe/CeO₂-O catalysts, a number of -OH species were formed through the dissociation of adsorbed H₂O molecules and accumulated at the oxygen vacancies on the CeO₂ surface [29]. These -OH species could block the reactive site and inhibit the activation and transfer of oxygen molecules, resulting in a decrease in propane oxidation activities. The PtFe/CeO₂-O catalyst possessed a high amount of oxygen vacancies and excellent oxygen mobility (discussed in the following sections), which led to a high H₂O resistance of the PtFe/CeO₂-O catalyst compared with the Pt/CeO₂ catalyst. When H₂O was removed, the C_3H_8 conversion was completely restored to its initial value and the C_3H_8 conversion on the Pt/CeO₂ and PtFe/CeO₂-O was completely restored to its initial value. Furthermore, no prominent deactivation was observed on PtFe/CeO₂-O catalyst during C_3H_8 oxidation, even in the presence of water vapour at 280 °C for 40 h

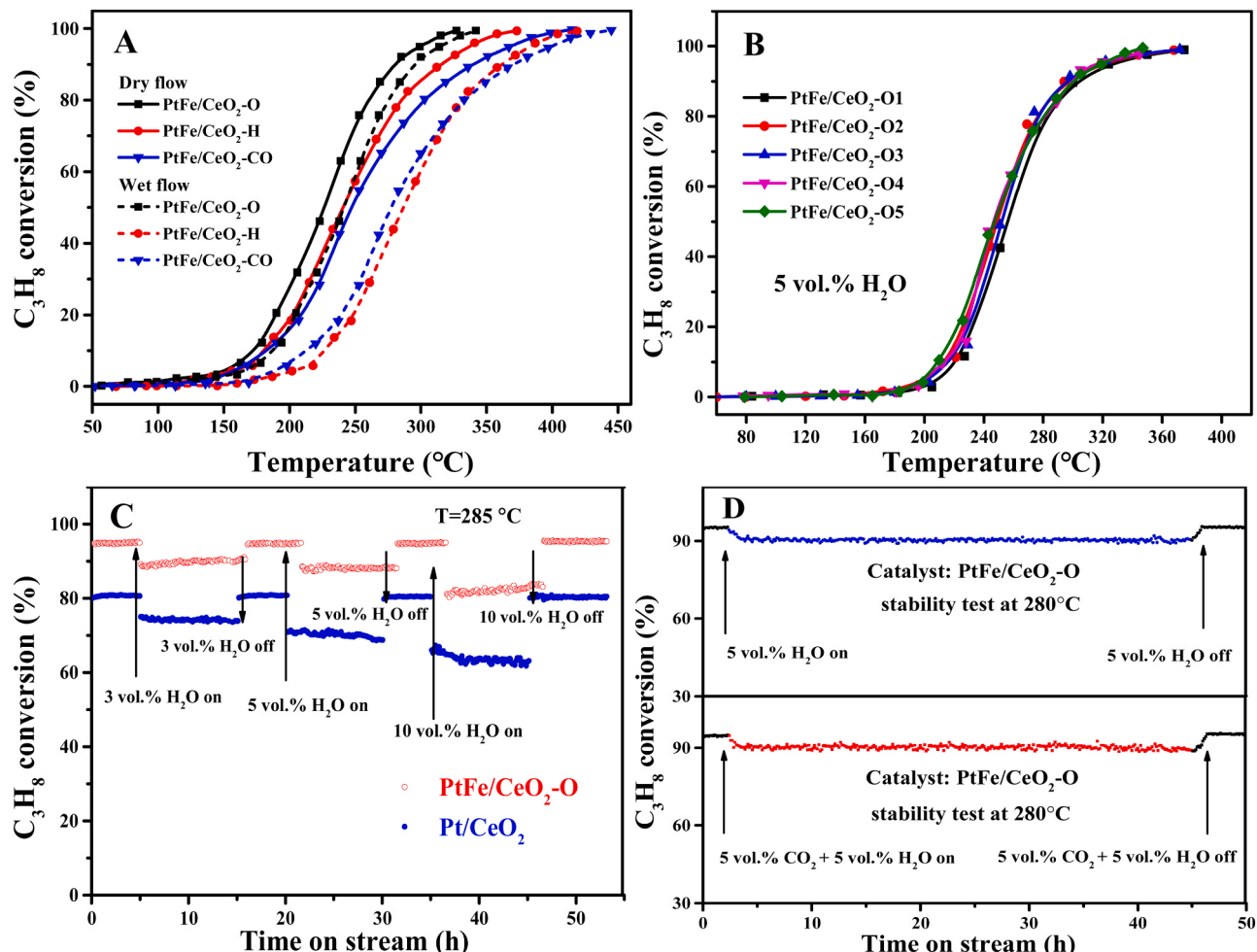


Fig. 2. (A) Light-off curves of the PtFe/CeO₂-x catalyst for C_3H_8 oxidation under dry and wet condition (5 vol% H₂O), (B) Recycling experiments of PtFe/CeO₂-O for C_3H_8 oxidation under humidity condition, (C) Effect of adding H₂O on C_3H_8 oxidation over the PtFe/CeO₂-O and Pt/CeO₂ catalysts at 285 °C, (D) The stability of PtFe/CeO₂-O for propane oxidation in the presence of CO₂ or H₂O. Reaction conditions: 0.2 vol% of C_3H_8 , 2 vol% of O₂, 3–10 vol% of H₂O (when used), Ar balanced, GHSV = 30000 mL·h⁻¹·g_{cat}⁻¹.

(Fig. 2D). The results demonstrated that PtFe/CeO₂-O exhibits excellent propane oxidation stability in humid or dry condition. More importantly, when feed gas containing 5 vol% H₂O and 5 vol% CO₂ was introduced together, the PtFe/CeO₂-O catalyst still displayed strong acid gas resistance (Fig. 2D). In short, these findings suggest that the PtFe/CeO₂-O catalyst is a suitable candidate for the removal of alkanes in industrial processes.

3.2. Structure evolution of PtFe nanoalloy

PtFe nanoalloys with similar sizes and shapes were prepared using a co-reduction-based colloidal chemistry method. The representative low-magnification TEM images of PtFe NPs as-synthesised at 300 °C are shown in Fig. S8A-B. The PtFe NPs were observed to be worm- or quasi-spherical in shape, with a diameter primarily ranging from 5.5 nm. In addition, compared with the XRD pattern for Pt NPs, the corresponding (111) peak of PtFe NPs shifted to a higher angle (Fig. S8E), which might

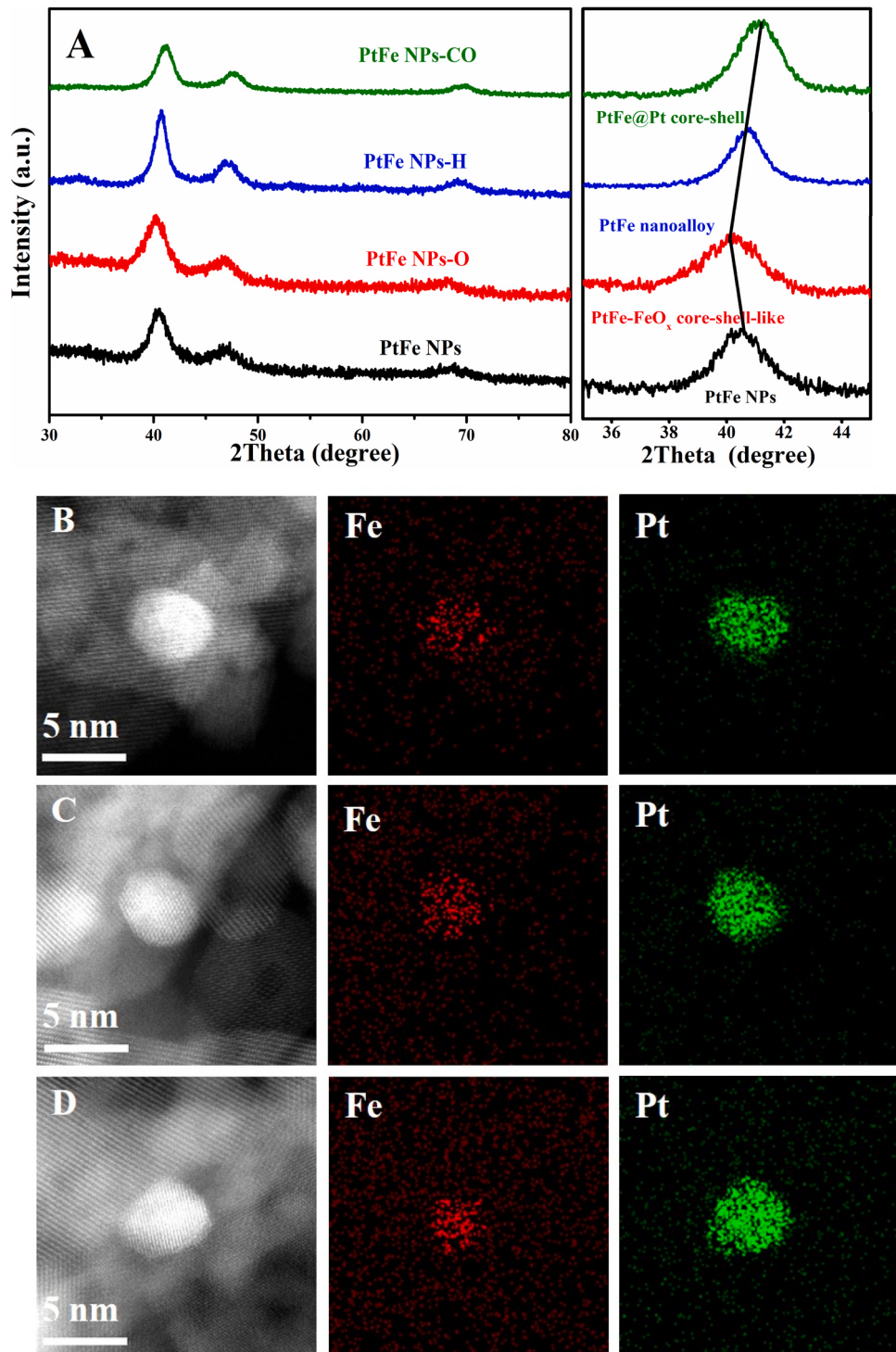


Fig. 3. (A) The XRD patterns of PtFe nanoalloy calcined under different atmospheres; STEM images and corresponding EDS elemental maps for the (B) PtFe/CeO₂-O, (C) PtFe/CeO₂-H and (D) PtFe/CeO₂-CO catalysts.

be attributable to the decrease in lattice spacing caused by the substitution of Fe atoms for Pt atoms [22]. More importantly, the XRD patterns of the PtFe NPs matched well with those of face-centred cubic (fcc) PtFe (PDF#29-0717). The average diameter of the PtFe nanoalloy calculated by the Scherrer equation was 4 nm, which was slightly smaller than the value obtained by TEM because of the nature of PtFe NPs polycrystals. Furthermore, the high-resolution TEM pictures of the PtFe NPs indicated a lattice fringe of 0.223 nm, and the FFT pattern showed clearly diffraction spots of the (111) planes of PtFe nanoalloy (Fig. S8C-D), consistent with the previous reports [22,27]. In brief, the PtFe nanoalloy with fcc structure, uniform size and morphology were successfully synthesised.

After deposition of the PtFe nanoalloy onto CeO₂, the PtFe/CeO₂ was pre-treated in different atmospheres to modulate the structure of the PtFe NPs and construct PtFe/CeO_{2-x} catalyst with different bimetallic structures. The grain size and specific surface area of the PtFe/CeO_{2-x} catalysts remained unchanged (Table S3). All the catalysts displayed only the fcc fluorite-type CeO₂ phase with the Fm-3 m (JCPDS 43-1002) space group (Fig. S9) [8]. The diffraction peaks of PtFe NPs, Pt, or Fe species were not observed in XRD pattern, indicating the high dispersion of the PtFe NPs on the CeO₂ support.

In general, the annealing treatment of bimetallic nanoalloy in different atmospheres can induce selective segregation of metal elements because of the different binding abilities of metal elements with adsorbent molecules [30–33]. Therefore, the XRD patterns of PtFe NPs calcined under different atmospheres were detected to investigate the segregation behaviour of Pt or Fe elements. As shown in Fig. 3A, all PtFe NPs demonstrated similar XRD patterns, and neither isolated Pt nor Fe species detected. There was a slight shift of the main peak assigned to PtFe NPs (111), indicating that the migration of metal elements occurred in the PtFe NPs rather than phase separation. After annealing in 20 vol% O₂/Ar, the (111) peak of PtFe shifted to a lower angle compared with pristine PtFe nanoalloy. It was noted that Fe, with a strong affinity for O₂, tended to diffuse out onto the PtFe NPs surface in the form of FeO_x species, leading to the enrichment of Fe element on PtFe NPs surface and a shift of the (111) peak to low 2θ as the smaller atomic radius of Fe than Pt [30,34]. Meanwhile, the diffused FeO_x species on the PtFe NPs should be amorphous nanoclusters rather than a compact shell, accompanied by a portion of exposed Pt atoms on the surface [20]. When the PtFe nanoalloy were annealed in CO atmosphere, the (111) peak of PtFe NPs shifted toward a higher angle compared with pristine PtFe nanoalloy, owing to the Pt species preferred to exsolve from the bulk phase of PtFe NPs to the surface due to the high adsorption enthalpy of CO on Pt compared to that on Fe. Consequently, the structure of PtFe NPs comprising a PtFe alloy core with a Pt shell was constructed after annealing in a CO atmosphere [35]. In contrast, the PtFe (111) peak of PtFe/CeO₂-H catalyst was kept unchanged compared with that of pristine PtFe NPs, indicating that the homogeneity of the PtFe nanoalloy was improved after annealing in 5 vol% H₂/Ar atmosphere [30].

The size and morphology of PtFe NPs on the surface of the PtFe/CeO_{2-x} catalysts after heat treatment with different atmospheres were characterized and the results were shown in Figs. 3B-D and S10. The size of PtFe NPs with worm- or quasi-spherical shapes on the PtFe/CeO_{2-x} catalyst was approximately 5 nm, indicating that post-treatment in O₂, H₂ or CO atmospheres did not induce significant changes in particle size and shape. Meanwhile, the size and morphology of PtFe NPs of the PtFe/CeO_{2-x} catalysts remained unchanged after oxidation reaction (Fig. S10). Furthermore, the unique structure of the PtFe NPs on the CeO₂ after annealing in different atmospheres was detected using aberration-corrected HAADF-STEM and STEM-EDS elemental mapping. On the PtFe/CeO₂-H catalyst, both Pt and Fe elements were found to be homogeneously distributed throughout the PtFe NPs. On the PtFe/CeO₂-CO catalyst, Pt and Fe were uniformly distributed in the majority of the PtFe NPs, and the surface layer was enriched with Pt. In contrast, Fe was enriched on the PtFe NPs surface of the PtFe/CeO₂-O catalyst. These findings aligned with the XRD results obtained for PtFe nanoalloys that

underwent calcination under varying atmospheric conditions.

In summary, the size, composition, and morphology of the PtFe NPs in the PtFe/CeO_{2-x} catalysts calcined under different atmospheres remained unchanged. However, the surface structure of the PtFe NPs was highly dependent on the post-treatment atmosphere. Specifically, the surface layer structure of PtFe NPs on the PtFe/CeO_{2-x} varied with the Pt skin shell, random distribution of Pt and Fe, and surface enrichment of amorphous FeO_x nanoclusters after annealing in CO, H₂/Ar, and O₂/Ar atmospheres using adsorbate-induced surface segregation.

3.3. Structure of catalysts and chemical state of Pt species

Based on the detection of the structural evolution of the PtFe nanoalloy after annealing the catalysts in different atmospheres, the structure of the catalysts and the chemical state of the Pt species were further characterised. First, FTIR was used to track variations in the oleylamine (OAm) molecules on the catalysts during the preparation process, and the results are shown in Fig. S11. Two weak peaks at 2923 and 2856 cm⁻¹ were observed for the pristine PtFe/CeO₂ sample, assigned to C-H bond stretches from OAm. However, those two peaks almost disappeared after extracting with the N₂H₄ solvents compared with pristine PtFe/CeO₂ samples, indicating the removal of capping agent of OAm [22].

The valence states of Pt and the surface composition of the PtFe/CeO_{2-x} catalysts were detected using XPS. According to Fig. 4A, the Pt 4 f signals of PtFe/CeO_{2-x} catalysts at 71.0–72.0 eV and 74.3–75.3 eV were attributed to metallic Pt 4 f_{7/2} and 4 f_{5/2}, respectively [13,36]. The main peak of Pt shifted from 71.3 eV in pristine PtFe/CeO₂ to 71.5 eV in PtFe/CeO₂-O. In contrast, the BE of Pt in PtFe/CeO₂-CO was shifted to a lower value (71.1 eV). As expected, the BE of Pt (71.2 eV) for the PtFe/CeO₂-H was comparatively close to that (71.3 eV) of Pt in pristine PtFe/CeO₂ due to the alloy structure of both the catalysts. Therefore, the results of Pt 4 f XPS demonstrated that the Pt species were primarily present in the metallic state for all PtFe/CeO_{2-x} catalysts. A CO-adsorption FTIR test was also performed on the catalysts to determine the state of the Pt species. In Fig. S12, the strong absorption peak was observed on the PtFe/CeO_{2-x} catalysts in comparison with pure CeO₂ support, which was attributed to the linear CO adsorbed on metallic Pt (CO-Pt⁰) [13]. Besides, the wavenumber of absorption peak decreased in the following order: PtFe/CeO₂-O (2088 cm⁻¹) > PtFe/CeO₂-H (2066 cm⁻¹) > PtFe/CeO₂-CO (2053 cm⁻¹), indicating that the sequence of the degree of electron deficiency of Pt on the PtFe/CeO_{2-x} catalysts was as follows: PtFe/CeO₂-O > PtFe/CeO₂-H > PtFe/CeO₂-CO. These results are in agreement with the Pt 4 f XPS spectra.

Fe 2p XPS spectra of the catalysts were shown in Fig. S13. It was noted that the two peaks at about 716 and 732 eV were assigned to Auger electron peak of Ce. The Fe 2p XPS was deconvoluted into Fe⁰ and Fe^{δ+} (2 < δ < 3) peaks [37], and the Fe⁰/(Fe⁰ + Fe^{δ+}) ratio was 8.4% for PtFe/CeO₂-O, 57.1% for PtFe/CeO₂-H and 35.3% for PtFe/CeO₂-CO, respectively. The high content of Fe^{δ+} on the surface of the PtFe/CeO₂-O catalyst was induced by the pretreatment in air atmosphere. However, the Fe^{δ+} species for the PtFe/CeO₂-H and PtFe/CeO₂-CO catalysts can be attributed to the interface between PtFe NPs and CeO₂ support, i.e. part of Fe atoms at the interface were oxidized by CeO₂.

In summary, the PtFe/CeO_{2-x} catalysts have Pt active sites of similar sizes and metallic states. However, the degree of electron deficiency of Pt over PtFe/CeO_{2-x} was different depending on the structure of the PtFe alloy.

3.4. Amount of active oxygen species

In General, the surface-chemisorbed oxygen species (O₂²⁻/O₂^{·-}), closely related to oxygen vacancies, mainly participate in the deep oxidation of intermediate species [5]. Besides, the redox properties of the catalyst, strongly associated with the surface-chemisorbed oxygen species and surface lattice oxygen (O²⁻), plays a vital role in oxidising performance

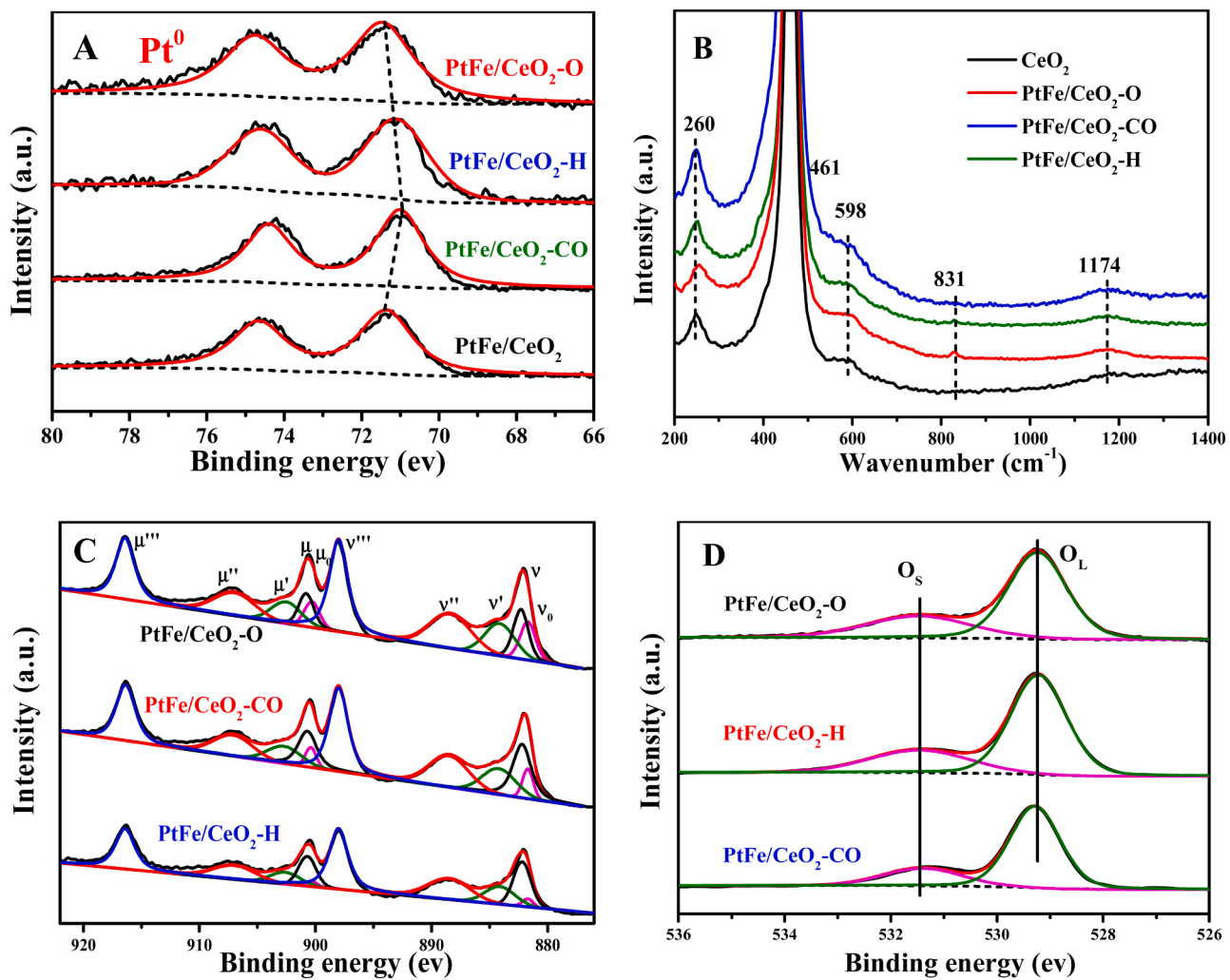


Fig. 4. (A) Pt 4f XPS, (B) Raman spectra, (C) Ce 3d and (D) O 1s XPS of the PtFe/CeO₂-x catalysts.

of the catalyst. Therefore, the surface-chemisorbed oxygen and redox properties of the PtFe/CeO₂-x catalyst were studied.

Firstly, the surface oxygen vacancies of the PtFe/CeO₂-x and CeO₂ were characterised by Raman spectra. In Fig. 4B, the CeO₂ sample exhibits four Raman signal peaks, include F_{2g} mode located at 461 cm⁻¹, second-order transverse acoustic mode at 260 cm⁻¹, defect-induced (D) mode at 598 cm⁻¹ and second-order longitudinal optical mode at 1174 cm⁻¹ [5]. After loading PtFe NPs, a new weak peak located at 831 cm⁻¹ was emerged for both PtFe/CeO₂-O and PtFe/CeO₂-H catalysts, assigned to peroxy-like species (O₂[·]) at oxygen vacancies [38]. Besides, the ratio of the D peak intensity to F_{2g} peak intensity (I_D/I_{F2g}) can reflect the relative amount of the surface oxygen vacancies [38]. Therefore, the I_D/I_{F2g} ratios of all catalysts were calculated and ranked in the order of PtFe/CeO₂-O (0.079) > PtFe/CeO₂-H (0.055) > PtFe/CeO₂-CO (0.051) > CeO₂ (0.028) (Table S4). Besides, the Ce 3d XPS spectra of PtFe/CeO₂-x catalyst were also obtained in Fig. 4C, the Ce 3d XPS spectra primarily composed of ten groups, including Ce⁴⁺ (v, v'', v'', u, u'', and u'') and Ce³⁺ (v₀, v', u₀, and u') [39,40]. Besides, the Ce³⁺/(Ce³⁺+Ce⁴⁺) values for the catalysts were calculated via peak area integration and followed the sequence: PtFe/CeO₂-O (26.3%) > PtFe/CeO₂-H (20.9%) > PtFe/CeO₂-CO (16.2%). The above results clearly prove that PtFe/CeO₂-O catalyst possessed the highest number of oxygen vacancies compared to the other catalysts, which could be attributed to the formation of Fe-O-Ce species in PtFe/CeO₂-O promoting the formation of oxygen vacancies at the CeO₂-FeO_x interface [37, 39].

Meanwhile, the nature of surface oxygen species on the PtFe/CeO₂-x catalysts was also detected using the O 1s XPS spectra (Fig. 4D). All of the PtFe/CeO₂-x catalysts showed a prominent peak at 529.2 eV, which corresponds to lattice oxygen (O_L). In addition, a shoulder peak at 531.4 eV was observed, which was assigned to surface chemisorbed oxygen species, hydroxyl groups, and adsorbed water molecules (O_S) [13,41]. The O_S/O_L values are shown in Table S4 and decreased in the order of PtFe/CeO₂-O (44.1%) > PtFe/CeO₂-H (34.7%) > PtFe/CeO₂-CO (30.1%). Combining the above results of the Raman, Ce 3d, and O 1s XPS spectra, it is concluded that the PtFe/CeO₂-O had the most surface-chemisorbed oxygen species owing to its abundance of oxygen vacancies, which were conducive to deeply oxidising the intermediate species during propane oxidation.

Finally, the redox performance of the catalysts, which are key parameters for propane oxidation, were determined by O₂-TPD and H₂-TPR. In Fig. 5A, an O₂-TPD experiment was carried out to identify the amount and mobility of reactive oxygen species (ROS) over the PtFe/CeO₂-x catalyst. The PtFe/CeO₂-H catalyst has a broad overlapping peak at 150–600 °C, attributed to the desorption of the surface chemisorbed oxygen (O₂[·]/O₂) and lattice oxygen (O²⁻) [8,13,42]. However, the oxygen desorption peak of the PtFe/CeO₂-O was observed at 250–550 °C. Similarly, the desorption curve of the PtFe/CeO₂-CO appeared at 250–550 °C, but its oxygen desorption peak intensity was markedly lower than that of the PtFe/CeO₂-O. The integrated peak areas were 3.82×10^{-10} , 1.76×10^{-10} and 9.51×10^{-11} for the PtFe/CeO₂-O, PtFe/CeO₂-H and PtFe/CeO₂-CO catalysts, respectively (Table S4). In

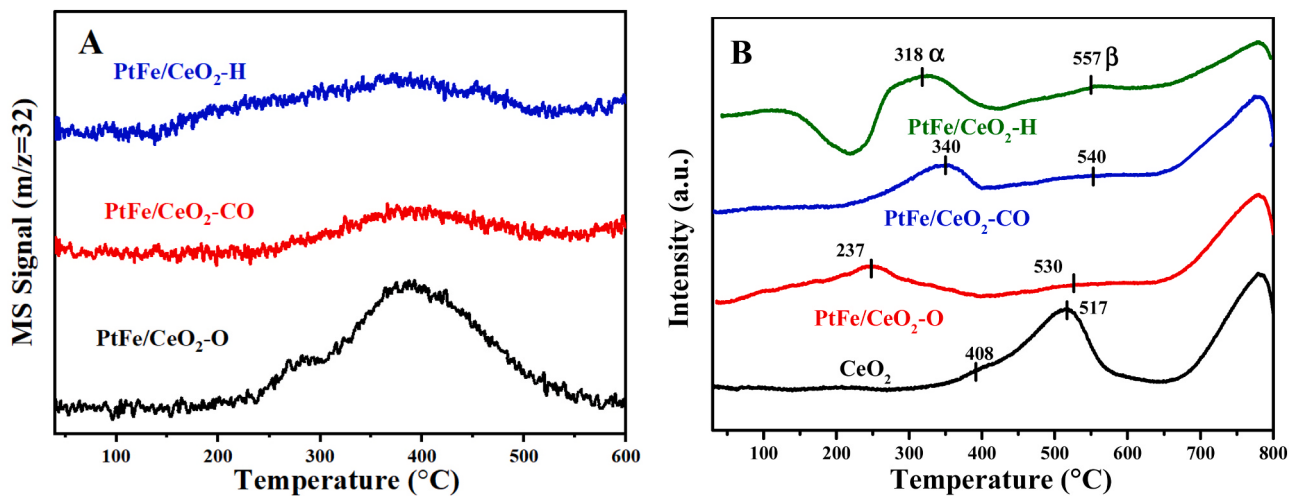


Fig. 5. (A) O₂-TPD, (B) H₂-TPR profiles of the PtFe/CeO₂-x catalysts.

addition, the first derivatives of O₂-TPD curves were calculated, and followed the sequence: PtFe/CeO₂-O (1.18×10^{-13}) > PtFe/CeO₂-H (5.62×10^{-14}) > PtFe/CeO₂-CO (4.33×10^{-14}). These results indicate that the PtFe/CeO₂-O catalyst has the highest amount of ROS and the highest oxygen release rate among all the catalysts.

H₂-TPR experiments were also carried out to evaluate the reducibility of the PtFe/CeO₂-x and CeO₂ samples (Fig. 5B). As for pure CeO₂ support, an overlapped and highly asymmetric peak appeared at 300–650 °C, which was assigned to the reduction of O₃ (408 °C, α) and O_L (515 °C, β) [38]. In contrast, the reduction peak α of PtFe/CeO₂-x catalysts significantly shifted to a low temperature, indicating that the PtFe NPs facilitated the reducibility of the CeO₂ support. Compared with the other two catalysts, an obvious negative peak located at 120–260 °C was found for the PtFe/CeO₂-H catalyst, due to the desorption of H₂ adsorbed on PtFe nanoalloy at low temperature [43]. As shown in the XPS results, Pt species were predominantly present in the metallic form over the PtFe/CeO₂-x catalysts. Therefore, the reduction peaks of PtFe/CeO₂-x were primarily caused by the reduction of surface-chemisorbed oxygen and surface Ce species derived by the hydrogen spillover from Pt to the CeO₂ support [37]. Further, the H₂ consumption of α peak for the PtFe/CeO₂-CO, PtFe/CeO₂-H and PtFe/CeO₂-O catalysts were 168, 217 and 520 $\mu\text{mol/g}$, respectively. These findings show that PtFe/CeO₂-O catalyst has superior redox properties

over the other two catalysts.

3.5. Propane adsorption and activation

In situ diffuse reflection infrared spectroscopy experiments were performed to investigate the ability of the PtFe/CeO₂-x catalysts to adsorb and oxidise the C₃H₈. The C₃H₈/Ar and C₃H₈/O₂/Ar feed gases were used for the adsorption and oxidation of C₃H₈. The adsorption and oxidation spectra of C₃H₈ on CeO₂ are similar (Fig. S14). Specifically, several peaks at 2985, 2965, 1569, 1536, 1465, 1395 and 1295 cm^{-1} were detected (Table S5). The peaks at 2985 and 2965 cm^{-1} are assigned to the stretching vibration of the C-H bond in chemisorbed propane, while the peaks at 1200–1800 cm^{-1} are typical oxygen-containing intermediate species, such as carboxylates and carbonates [44], indicating that the propane molecule could be adsorbed on CeO₂ and subsequently oxidised by the active oxygen species.

In the process of propane adsorption (Fig. 6A), the intensities of peaks at 1200–1800 cm^{-1} for the PtFe/CeO₂-x catalysts were obviously higher than those for the CeO₂ support. Several peaks at 1575, 1543, 1474, 1430, 1396, 1356, and 1318 cm^{-1} appeared for formate (1575, 1356 cm^{-1}), acetate (1474 cm^{-1}), carbonate (1543, 1318 cm^{-1}), and methyl species (1396 cm^{-1}) [13, 44]. Although more accessible metallic Pt sites were available on the PtFe/CeO₂-CO, the peak intensity

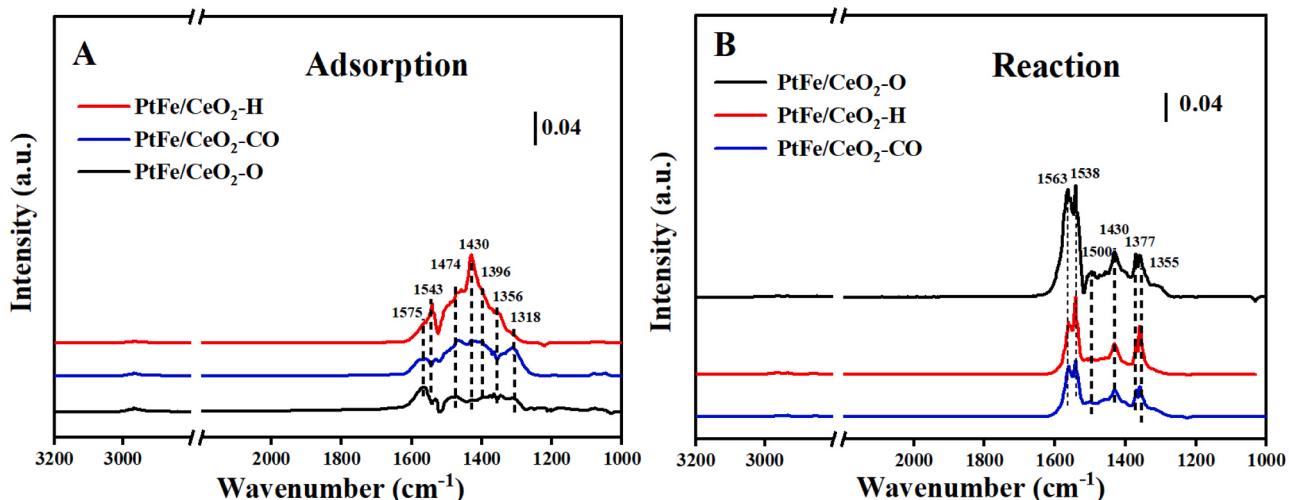


Fig. 6. (A) In situ DRIFT spectra for C₃H₈ adsorption (0.2 vol% of C₃H₈ balanced with 99.8 vol% Ar) and (B) reaction (0.2 vol% C₃H₈ and 2 vol% O₂ balanced with 97.8 vol% Ar) over PtFe/CeO₂-x catalysts at 280 °C.

for the PtFe/CeO₂-H catalyst was higher than those of PtFe/CeO₂-CO catalyst. As shown in CO-FTIR results, the metal Pt species of the PtFe/CeO₂-H catalyst were in a more electron-deficient state than those of the PtFe/CeO₂-CO catalyst, which benefited the activation of propane molecules and led to high peak intensities for the PtFe/CeO₂-H [19,45]. In contrast, the peak intensities for the PtFe/CeO₂-O catalyst were the weakest because the FeO_x nanoclusters present on PtFe NPs core surface can reduce the availability of Pt active sites, resulting in the inhibition of propane adsorption [29].

When the feed gas was changed to a mixture of C₃H₈, O₂ and Ar, the spectra of C₃H₈ oxidation on all catalysts drastically changed compared to those of C₃H₈ adsorption (Fig. 6B). The intensities of the peaks at 1200–1800 cm⁻¹ on all the catalysts markedly increased compared to that in the spectra of C₃H₈ adsorption, indicating that the PtFe/CeO₂-x catalysts became more effective in adsorbing and activating propane in the presence of oxygen. Among the three catalysts, the PtFe/CeO₂-O catalyst demonstrated the strongest intensities of peaks related to the oxidised intermediate species compared to the PtFe/CeO₂-H and PtFe/CeO₂-CO catalysts, owing to the highest amount of surface-chemisorbed oxygen species on the PtFe/CeO₂-O catalyst.

Additionally, the evolution of the intermediate species between C₃H₈ oxidation and adsorption was dependent on the PtFe/CeO₂-x catalyst owing to their different redox performances. For the PtFe/CeO₂-O catalyst, the intermediate species, including formate (1563, 1355 cm⁻¹) and carbonate species (1538 cm⁻¹), was dominant during both C₃H₈ oxidation and adsorption (Fig. S15). However, the oxygen-containing intermediate species over PtFe/CeO₂-H and PtFe/CeO₂-CO in the process of propane oxidation changed significantly compared with those during adsorption. The acetate species (1474 and 1430 cm⁻¹) during adsorption on the both catalysts were further oxidised into formate (1563 and 1355 cm⁻¹) and carbonate species (1538 cm⁻¹) during the oxidation process (Fig. S16–17). Meanwhile, combined the DRIFT results with our previous work [8,13], it is inferred that the propane oxidation path on the PtFe/CeO₂-x catalysts all followed: propane → propionate → formate/acetate → carbonate → CO₂ and H₂O.

3.6. Discussion

PtFe/CeO₂-x catalysts with similar sizes, compositions and morphologies, but variable surface structures of PtFe NPs, were prepared through adsorbate-induced surface segregation. Specifically, after thermal treatment under an O₂ atmosphere, the structure of the PtFe NPs on the PtFe/CeO₂-O catalyst consisted of dispersed FeO_x nanoclusters anchored on the PtFe NPs core. However, after thermal treatment under a CO atmosphere, the Pt atoms were enriched on the surface of the PtFe NPs because of the stronger binding of the Pt atoms to CO than to the Fe atoms, leading to a Pt shell around the PtFe core on the PtFe/CeO₂-CO catalyst. In contrast, only the alloying degree of PtFe NPs was further increased after calcination under 5 vol% H₂/Ar gas, without the segregation of Pt or Fe elements for the PtFe/CeO₂-H catalyst.

Generally, propane oxidation over the PtFe/CeO₂-x catalysts followed the MvK mechanism, in which propane was adsorbed on the catalyst and the first C-H bond was dissociated on the Pt active sites. The hydrocarbon fragments were then completely oxidised to CO₂ and H₂O by the ROS on the catalyst, along with the formation of surface oxygen vacancies, which were subsequently replenished by gas-phase O₂ [46–48]. Therefore, both the adsorption of propane and the activation of O₂ are critical factors in determining the propane catalytic oxidation performance of catalysts.

The Pt species were in a metallic state on all PtFe/CeO₂-x catalysts, but the number of available Pt active sites differed among the PtFe/CeO₂-x catalysts based on the PtFe NPs structures. The PtFe/CeO₂-H catalyst exhibited the highest propane adsorption ability, followed by the PtFe/CeO₂-CO and PtFe/CeO₂-O catalysts, which was also confirmed by C₃H₈-TPD results (Fig. S18). However, the ability of the PtFe/CeO₂-x catalyst to adsorb propane is inconsistent with the order of its activity

for C₃H₈ oxidation. Instead, the amount of intermediate species in the DRIFT spectra of C₃H₈ oxidation suggests a positive relationship with their activity for C₃H₈ oxidation (Fig. 6B). These results demonstrate that the Pt active sites for C₃H₈ adsorption and C-H bond cleavage were sufficient for all PtFe/CeO₂-x catalysts, and their activities for C₃H₈ oxidation were dependent on the quantity of reactive oxygen species in the catalysts.

As shown in Fig. 7A, the TOF values of the C₃H₈ oxidation over PtFe/CeO₂-x catalysts at 200 °C were positively correlated with the concentration of oxygen vacancies (I_D/I_{F2g}) and the amount of active oxygen species (O₂-TPD and O_S/O_T) on the catalyst surface. The PtFe/CeO₂-O catalyst had the most surface-chemisorbed oxygen species because of its large number of oxygen vacancies over the catalyst, which was conducive to the deep oxidation of the intermediate species during propane oxidation. In addition, PtFe/CeO₂-O possessed the best redox properties compared to the other two catalysts, including the most abundant activated oxygen species (surface-chemisorbed oxygen and surface lattice oxygen species) and the highest oxygen release rate among all catalysts, which led to significantly higher activity in propane oxidation compared to the PtFe/CeO₂-H and PtFe/CeO₂-CO catalysts.

To further elucidate the role of the FeO_x species in the PtFe/CeO₂-O for propane oxidation, a monometallic Pt/CeO₂ catalyst was synthesised by loading Pt NPs with a size of approximately 4.5 nm onto a CeO₂ support (Fig. S19). The ability of Pt/CeO₂ catalyst to oxidise propane was significantly lower than that of PtFe/CeO₂-O, indicating that the dispersed FeO_x patches anchored to the PtFe core functioned as an oxygen reservoir for oxygen activation (Fig. 7B) [49]. Meanwhile, the propane activity of the PtFe/SiO₂-O catalyst was also higher than those of the PtFe/SiO₂-CO and PtFe/SiO₂-H catalysts, confirming the positive role of the FeO_x species on the PtFe core (Fig. S20). More importantly, the propane oxidation activities of the Pt/CeO₂-IMP, Fe/CeO₂-IMP, PtFe/CeO₂-IMP and PtFe/CeO₂-IMP-R catalysts prepared by incipient wetness impregnation method were significantly inferior to that of the PtFe/CeO₂-O catalyst, highlighting the better synergistic effect of Pt and Fe over PtFe/CeO₂-O in propane oxidation.

Therefore, the PtFe/CeO₂-O catalyst gave the best catalytic performance for oxidising propane, primarily because Pt species remained in the metallic state and possessed a strong ability to cleave the C-H bond. In addition, the strong interaction between FeO_x and CeO₂ leads to an abundance of ROS formed on the catalyst. Meanwhile, the FeO_x species bonded to the PtFe NPs surface also functioned as additional sites for oxygen adsorption and activation. In addition to propane, this method of optimising PtFe NPs structure can be used to improve oxidation efficiency of other VOCs, such as toluene (Fig. S21).

4. Conclusion

The PtFe nanoalloy were successfully prepared using a colloidal chemical method, and their structures and surface compositions were effectively regulated using an adsorbate-induced surface segregation strategy. The synthesised PtFe alloy NPs evolved into PtFe-FeO_x core-shell-like, PtFe nanoalloy, and PtFe@Pt core-shell structures after calcination under O₂/Ar, H₂/Ar, and CO atmospheres, respectively. Besides, the size, composition, and morphology of the PtFe NPs in the PtFe/CeO₂-x catalysts remained unchanged, and the Pt species are mainly in the metallic state. In the oxidation of propane, the PtFe/CeO₂-O catalyst exhibited higher activity, resistance to H₂O, and stability in comparison to the PtFe/CeO₂-H and PtFe/CeO₂-CO catalysts, and even the propane oxidation rate and TOF for the PtFe/CeO₂-O were higher than those of most catalysts reported in the literature. On the other hand, the formation of PtFe-FeO_x core-shell-like in the PtFe/CeO₂-O catalyst promoted the formation of oxygen vacancies on the catalyst. As a result, the PtFe/CeO₂-O catalyst possessed the most surface-chemisorbed oxygen species, which greatly facilitated deep oxidation of intermediate species in propane oxidation. Meanwhile, the PtFe/CeO₂-O catalyst showed the best redox properties among all catalysts,

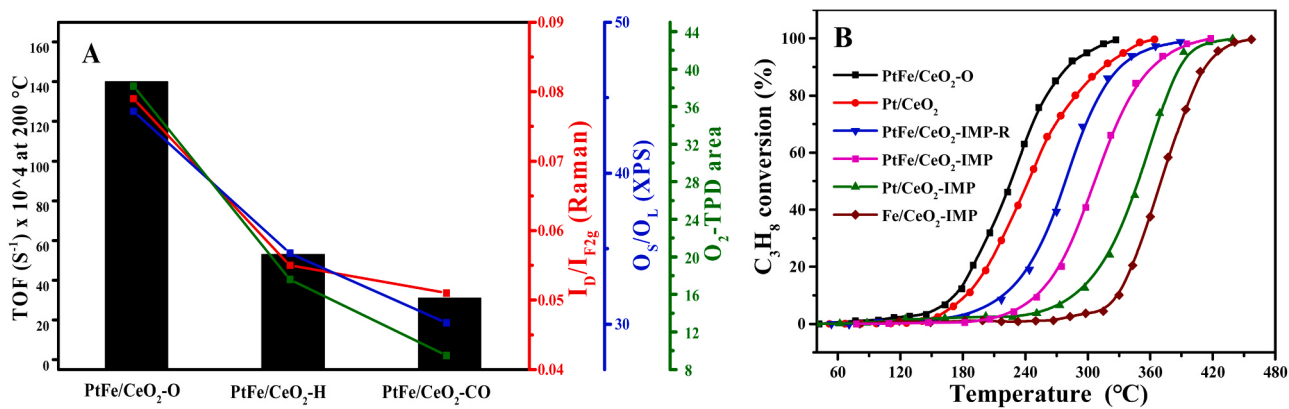


Fig. 7. (A) Correlation between TOF (at 200 °C) and oxygen vacancies concentration (Raman results) and the amount of active oxygen species (XPS and O₂-TPD results) over the PtFe/CeO₂-x catalysts, (B) The catalytic activities of the PtFe/CeO₂-O, Pt/CeO₂, PtFe/CeO₂-IMP-R, PtFe/CeO₂-IMP, Pt/CeO₂-IMP, and Fe/CeO₂-IMP catalysts for propane oxidation. (Reaction condition: 0.2 vol% C₃H₈, 2 vol% O₂, Ar balanced, and GHSV of 30000 mL·h⁻¹·g_{cat}⁻¹).

including the most abundant reactive oxygen species (surface-chemisorbed oxygen and surface lattice oxygen) and the highest oxygen release rate, resulting in the highest activity in propane oxidation. This study provides a promising strategy for the rational design of highly active and water-resistant Pt catalysts for the elimination of VOCs pollutants.

CRediT authorship contribution statement

Zhenpeng Huang: Conceptualization, Methodology, Data curation, Investigation, Writing – original draft. **Jihang Yu:** Investigation, Methodology, Validation, Writing – review & editing. **Wenbo Li:** Methodology, Writing – review & editing. **Xuan Tang:** Methodology, Writing – review & editing. **Yanglong Guo:** Supervision, Formal analysis, Writing – review & editing. **Yun Guo:** Supervision, Formal analysis, Writing – review & editing. **Li Wang:** Supervision, Formal analysis, Writing – review & editing. **Sheng Dai:** Writing – review & editing. **Rui Liu:** Writing – review & editing. **Wangcheng Zhan:** Supervision, Funding acquisition, Writing – review & editing.

Declaration of Competing Interest

The authors declare that they have no known competing financial interests or personal relationships that could have appeared to influence the work reported in this paper.

Data availability

No data was used for the research described in the article.

Acknowledgments

Z.H. and W.Z. acknowledge financial support from the National Key Research and Development Program (2022YFB3504200) and the National Natural Science Foundation of China (21922602, 22076047). Y.G. thanks the National Natural Science Foundation of China (U21A20326). Y.G. and L.W. thanks the Shanghai Science and Technology Innovation Action Plan (20dz1204200) and Fundamental Research Funds for the Central Universities. R.L. thanks the National Natural Science Foundation of China (22276209).

Appendix A. Supplementary data

The characterisation details and activity test are supplied along with the ICP data, XRD patterns, in situ DRIFTS spectra, catalytic activity data and related table. The [supporting information](#) is freely available on the

ACS Publications website.

Appendix B. Supporting information

Supplementary data associated with this article can be found in the online version at [doi:10.1016/j.apcatb.2023.123198](https://doi.org/10.1016/j.apcatb.2023.123198).

References

- C. He, J. Cheng, X. Zhang, M. Douthwaite, S. Pattison, Z. Hao, Recent advances in the catalytic oxidation of volatile organic compounds: A review based on pollutant sorts and sources, *Chem. Rev.* 119 (2019) 4471–4568.
- H. Liu, X. Li, Q. Dai, H. Zhao, G. Chai, Y. Guo, Y. Guo, L. Wang, W. Zhan, Catalytic oxidation of chlorinated volatile organic compounds over Mn-Ti composite oxides catalysts: Elucidating the influence of surface acidity, *Appl. Catal. B Environ.* 282 (2021) 11957–11966.
- R. Peng, S. Li, X. Sun, Q. Ren, L. Chen, M. Fu, J. Wu, D. Ye, Size effect of Pt nanoparticles on the catalytic oxidation of toluene over Pt/CeO₂ catalysts, *Appl. Catal. B Environ.* 220 (2018) 462–470.
- Y. Guo, M. Wen, G. Li, T. An, Recent advances in VOC elimination by catalytic oxidation technology onto various nanoparticles catalysts: a critical review, *Appl. Catal. B Environ.* 281 (2021), 119447.
- Y. Fang, L. Li, J. Yang, S. Hoang, L. Wang, J. Xu, W. Yang, C. Pan, Y. Zhu, H. Deng, Z. Luo, C. Sun, D. Gao, Z. Li, Y. Guo, Engineering the nucleophilic active oxygen species in CuTiO_x for efficient low-temperature propene combustion, *Environ. Sci. Technol.* 54 (2020) 15476–15488.
- G. Chai, W. Zhang, L.F. Liotta, M. Li, Y. Guo, A. Giroir-Fendler, Total oxidation of propane over Co₃O₄-based catalysts: Elucidating the influence of Zr dopant, *Appl. Catal. B Environ.* 298 (2021), 120606.
- C. Feng, Q. Gao, G. Xiong, Y. Chen, Y. Pan, Z. Fei, Y. Li, Y. Lu, C. Liu, Y. Liu, Defect engineering technique for the fabrication of LaCo₃ perovskite catalyst via urea treatment for total oxidation of propane, *Appl. Catal. B Environ.* 304 (2022), 121005.
- Z. Huang, S. Cao, J. Yu, X. Tang, Y. Guo, Y. Guo, L. Wang, S. Dai, W. Zhan, Total oxidation of light alkane over phosphate-modified Pt/CeO₂ Catalysts, *Environ. Sci. Technol.* 56 (2022) 9661–9671.
- G. Li, N. Li, Y. Sun, Y. Qu, Z. Jiang, Z. Zhao, Z. Zhang, J. Cheng, Z. Hao, Efficient defect engineering in Co-Mn binary oxides for low-temperature propane oxidation, *Appl. Catal. B Environ.* 282 (2021), 119512.
- W. Liu, S. Yang, Q. Zhang, T. He, Y. Luo, J. Tao, D. Wu, H. Peng, Insights into flower-like Al₂O₃ spheres with rich unsaturated pentacoordinate Al³⁺ sites stabilizing Ru-CeO_x for propane total oxidation, *Appl. Catal. B Environ.* 292 (2021), 120171.
- H. Hao, B. Jin, W. Liu, X. Wu, F. Yin, S. Liu, Robust Pt@TiO_x/TiO₂ catalysts for hydrocarbon combustion: Effects of Pt-TiO_x interaction and sulfates, *ACS Catal.* 10 (2020) 13543–13548.
- Y. Fang, H. Li, Q. Zhang, C. Wang, J. Xu, H. Shen, J. Yang, C. Pan, Y. Zhu, Z. Luo, Y. Guo, Oxygen vacancy-governed opposite catalytic performance for C₂H₆ and C₃H₈ combustion: The effect of the Pt electronic structure and chemisorbed oxygen species, *Environ. Sci. Technol.* 56 (2022) 3245–3257.
- Z. Huang, J. Ding, X. Yang, H. Liu, P. Song, Y. Guo, Y. Guo, L. Wang, W. Zhan, Highly efficient oxidation of propane at low temperature over a Pt-based catalyst by optimization support, *Environ. Sci. Technol.* 56 (2022) 17278–17287.
- C. O'Brien, G. Jenness, H. Dong, D. Vlachos, I. Lee, Deactivation of Pt/Al₂O₃ during propane oxidation at low temperatures: Kinetic regimes and platinum oxide formation, *J. Catal.* 337 (2016) 122–132.

[15] K. Adamskaa, J. Okal, W. Tylus, Stable bimetallic Ru-Mo/Al₂O₃ catalysts for the light alkane combustion: Effect of the Mo addition, *Appl. Catal. B Environ.* 246 (2019) 180–194.

[16] W. Liao, Y. Liu, P. Zhao, B. Cen, C. Tang, A. Jia, J. Lu, M. Luo, Total oxidation of propane over Pt-V/SiO₂ catalysts: Remarkable enhancement of activity by vanadium promotion, *Appl. Catal. A Gen.* 590 (2020) 117337–117346.

[17] W. Liao, X. Fang, B. Cen, J. Chen, Y. Liu, M. Luo, J. Lu, Deep oxidation of propane over WO₃-promoted Pt/BN catalysts: The critical role of Pt-WO₃ interface, *Appl. Catal. B Environ.* 272 (2020) 118858–118867.

[18] P. Zhao, X. Li, W. Liao, Y. Wang, J. Chen, J. Lu, M. Luo, Understanding the role of NbO_x on Pt/Al₂O₃ for effective catalytic propane oxidation, *Ind. Eng. Chem. Res.* 58 (2019) 21945–21952.

[19] N. Tahsini, A. Yang, V. Streibel, B. Wergli, E. Goodman, A. Aitbekova, S. Bare, Y. Li, P. Abild-Pedersen, M. Cargnello, Colloidal platinum-copper nanocrystal alloy catalysts surpass platinum in low-temperature propene combustion, *J. Am. Chem. Soc.* 144 (2022) 1612–1621.

[20] X. Liu, Z. Hood, Q. Zheng, T. Jin, G. Foo, Z. Wu, C. Tian, Y. Guo, S. Dai, W. Zhan, H. Zhu, M. Chi, Optimizing the structural configuration of FePt-FeO_x nanoparticles at the atomic scale by tuning the post-synthetic conditions, *Nano Energy* 55 (2019) 441–446.

[21] C. Wang, M. Chi, D. Li, D. Strmcnik, D. van der Vliet, G. Wang, V. Komanicky, K. Chang, A. Paulikas, D. Tripkovic, J. Pearson, K. More, N. Markovic, V. Stamenkovic, Design and synthesis of bimetallic electrocatalyst with multilayered Pt-skin surfaces, *J. Am. Chem. Soc.* 133 (2011) 14396–14403.

[22] H. Zhu, Z. Wu, D. Su, G. Veith, H. Lu, P. Zhang, S. Choi, S. Dai, Constructing hierarchical interfaces: TiO₂-supported PtFe-FeO_x nanowires for room temperature CO oxidation, *J. Am. Chem. Soc.* 137 (2015) 10156–10159.

[23] S. Shan, J. Li, Y. Maswadeh, C. O'Brien, H. Kareem, D. Tran, I. Lee, Z. Wu, S. Wang, S. Yan, H. Cronk, D. Mott, L. Yang, J. Luo, V. Petkov, C. Zhong, Surface oxygenation of multicomponent nanoparticles toward active and stable oxidation catalysts, *Nat. Commun.* 11 (2020) 4201–4210.

[24] X. Xu, Q. Fu, X. Guo, X. Bao, A highly active “NiO-on-Au” surface architecture for CO oxidation, *ACS Catal.* 3 (2013) 1810–1818.

[25] Z. Yan, B. Yao, C. Hall, Q. Gao, W. Zang, H. Zhou, Q. He, H. Zhu, Metal-metal oxide catalytic interface formation and structural evolution: A discovery of strong metal-support bonding, ordered intermetallics, and single atoms, *Nano Lett.* 22 (2022) 8122–8129.

[26] M. Chi, C. Wang, Y. Lei, G. Wang, D. Li, K. More, A. Lupini, L. Allard, N. Markovic, V. Stamenkovic, Surface faceting and elemental diffusion behaviour at atomic scale for alloy nanoparticles during *in situ* annealing, *Nat. Commun.* 6 (2015) 8925–8933.

[27] Y. Yu, W. Yang, X. Sun, W. Zhu, X. Li, D. Sellmyer, S. Sun, Monodisperse MPt (M = Fe, Co, Ni, Cu, Zn) nanoparticles prepared from a facile oleylamine reduction of metal salts, *Nano Lett.* 14 (2014) 2778–2782.

[28] M. Chen, J. Kim, J. Liu, H. Fan, S. Sun, Synthesis of FePt nanocubes and their oriented self-assembly, *J. Am. Chem. Soc.* 128 (2006) 7132–7133.

[29] W. Schwartz, D. Ciuparu, L. Pfefferle, Combustion of methane over palladium-based catalysts: catalytic deactivation and role of the support, *J. Phys. Chem. C.* 116 (2012) 8587–8593.

[30] Z. Liu, G. Jackson, B. Eichhorn, Tuning the CO-tolerance of Pt-Fe bimetallic nanoparticle electrocatalysts through architectural control, *Energy Environ. Sci.* 4 (2011) 1900–1903.

[31] Y. Wu, Y. Li, S. Han, M. Li, W. Shen, Atomic-scale engineering of CuO_x-Au interfaces over AuCu single-nanoparticles, *ACS Appl. Mater. Interfaces* 14 (2022) 55644–55652.

[32] L. Wang, D. Johnson, Predicted trends of core-shell preferences for 132 late transition-metal binary-alloy nanoparticles, *J. Am. Chem. Soc.* 131 (2009) 14023–14029.

[33] J. Chen, X. Lv, W. Xu, X. Li, J. Chen, H. Jia, Utilizing Cl coordination to facilitate Ru-Ag self-assembling into alloy and recover thermally-inactivated catalyst for propane combustion, *Appl. Catal. B Environ.* 290 (2021), 119989.

[34] R. Mu, X. Guo, Q. Fu, X. Bao, Oscillation of surface structure and reactivity of PtNi bimetallic catalysts with redox treatments at variable temperatures, *J. Phys. Chem. C.* 115 (2011) 20590–20595.

[35] K. Mayrhofer, V. Juhart, K. Hartl, M. Hanzlik, M. Arenz, Adsorbate-induced surface segregation for core-shell nanocatalysts, *Angew. Chem. Int. Ed.* 48 (2009) 3529–3531.

[36] Q. Wang, S. Chen, F. Shi, K. Chen, Y. Nie, Y. Wang, R. Wu, J. Li, Y. Zhang, W. Ding, Y. Li, L. Li, Z. Wei, Structural evolution of solid Pt nanoparticles to a hollow PtFe alloy with a Pt-skin surface via space-confined pyrolysis and the nanoscale kirkendall effect, *Appl. Mater.* 28 (2016) 10673–10678.

[37] S. Song, Y. Wu, S. Ge, L. Wang, Y. Wang, Y. Guo, W. Zhan, Y. Guo, A facile way to improve Pt atom efficiency for CO oxidation at low temperature: Modification by transition metal oxides, *ACS Catal.* 9 (2019) 6177–6187.

[38] Y. Gu, T. Cai, X. Gao, H. Xia, W. Sun, J. Zhao, Q. Dai, X. Wang, Catalytic combustion of chlorinated aromatics over WO_x/CeO₂ catalysts at low temperature, *Appl. Catal. B Environ.* 248 (2019) 264–276.

[39] H. Li, K. Li, H. Wang, X. Zhu, Y. Wei, D. Yan, X. Cheng, K. Zhai, Soot combustion over Ce_{1-x}Fe_xO_{2-x} and CeO₂/Fe₂O₃ catalysts: Roles of solid solution and interfacial interactions in the mixed oxides, *Appl. Surf. Sci.* 390 (2016) 513–525.

[40] J. Luo, M. Meng, J. Yao, X. Li, Y. Zha, X. Wang, T. Zhang, One-step synthesis of nanostructured Pd-doped mixed oxides MO_x-CeO₂ (M=Mn, Fe, Co, Ni, Cu) for efficient CO and C₃H₈ total oxidation, *Appl. Catal. B Environ.* 87 (2009) 92–103.

[41] Y. Jian, M. Tian, C. He, J. Xiong, Z. Jiang, H. Jin, L. Zheng, R. Albilali, J.W. Shi, Efficient propane low-temperature destruction by Co₃O₄ crystal facets engineering: Unveiling the decisive role of lattice and oxygen defects and surface acid-base pairs, *Appl. Catal. B Environ.* 283 (2021) 119657.

[42] C. Schilling, M. Ganduglia-Pirovano, C. Hess, Experimental and theoretical study on the nature of adsorbed oxygen species on shaped ceria nanoparticles, *J. Phys. Chem. Lett.* 9 (2018) 6593–6598.

[43] Q. Fu, Y. Yao, X. Guo, M. Wei, Y. Ning, H. Liu, F. Yang, Z. Liu, X. Bao, Reversible structural transformation of FeO_x nanostructures on Pt under cycling redox conditions and its effect on oxidation catalysis, *Phys. Chem. Chem. Phys.* 15 (2013) 14708–14714.

[44] Z. Hu, Z. Wang, Y. Guo, L. Wang, Y. Guo, J. Zhang, W. Zhan, Total oxidation of propane over a Ru/CeO₂ catalyst at low temperature, *Environ. Sci. Technol.* 52 (2018) 9531–9541.

[45] A. Tomita, T. Miki, Y. Tai, Effect of water treatment and Fe doping on Pt sintering and the propane oxidation activity of Pt/Al₂O₃, *Appl. Catal. A Gen.* 522 (2016) 138–144.

[46] H. Luo, X. Wu, D. Weng, S. Liu, R. Ran, A novel insight into enhanced propane combustion performance on Pt/USY catalyst, *Rare Met.* 36 (2017) 1–9.

[47] W. Zhu, X. Chen, J. Jin, X. Di, C. Liang, Z. Liu, Insight into catalytic properties of Co₃O₄-CeO₂ binary oxides for propane total oxidation, *Chin. J. Catal.* 41 (2020) 679–690.

[48] K.A. Ledwa, M. Pawlyta, L. Kepinski, Ru_xCe_{1-x}O_{2-y} nanoparticles deposited on functionalized γ -Al₂O₃ as a thermally stable oxidation catalyst, *Appl. Catal. B Environ.* 230 (2018) 135–144.

[49] I. Ro, I. Aragao, J. Chada, Y. Liu, K. Rivera-Dones, M. Ball, D. Zanchet, J. Dumesic, G. Huber, The role of Pt-Fe_xO_y interfacial sites for CO oxidation, *J. Catal.* 358 (2018) 19–26.